CRYSTAL GROWTH & DESIGN

Article

pubs.acs.org/crystal

Single-Crystal-to-Single-Crystal Transformation of a Novel 2-Fold Interpenetrated Cadmium-Organic Framework with Trimesate and 1,2-Bis(4-pyridyl)ethane into the Thermally Desolvated Form Which Exhibits Liquid and Gas Sorption Properties

Ahmad Husain,[†] Mario Ellwart,[‡] Susan A. Bourne,[†] Lars Öhrström,[§] and Clive L. Oliver*[,†]

[†]Centre for Supramolecular Chemistry Research, Department of Chemistry, University of Cape Town, Rondebosch, 7701, South Africa

[‡]Department of Chemistry, Ludwig-Maximilians-Universität, München, Germany

[§]Chemical and Biological Engineering, Physical Chemistry, Chalmers University of Technology, Kemivägen 10, Göteborg, Sweden

Supporting Information

ABSTRACT: A novel 2-fold interpenetrated, pillared, cadmium metal−organic framework, namely, $[Cd(HBTC)BPE]_n \cdot n$DMF, has been synthesized using 1,3,5-benzenetricarboxylic acid and 1,2-bis(4-pyridyl)ethane (BPE). This compound has been desolvated and subjected to various liquids and gases for sorption studies. Structures of the as-synthesized (**1**), desolvated (**2**), and resolvated in benzene (**3**) have been determined by single-crystal X-ray diffraction analysis and further characterized by elemental analysis, IR spectra, and thermogravimetric/differential scanning calorimetry analysis. Single crystal X-ray analysis revealed a 2-fold interpenetrated, three-dimensional (3D) framework which exhibits a 3,5-connected network with the Schläfli symbol of $[(6^3)(6^9.8)]$ and *hms* topology. Compound **1** exhibits a temperature-induced single-crystal-to-single-crystal (SC−SC) transformation upon the release of *N*,*N*′-dimethylformamide molecules forming compound **2** (stable up to 300 °C). SC−SC transformation is also observed when it is immersed in benzene, chloroform, 1,4-dioxane, and tetrahydrofuran. The uptake of different solvent molecules was analyzed, and desolvated samples selectively adsorb benzene, chloroform, 1,4-dioxane, and THF molecules over other selected polar solvents. Gas (N_2, CO_2, and N_2O) sorption experiments were also performed and the structure showed 2.5% N_2, 4.5% CO_2, and 3.4% N_2O absorption by mass at room temperature and moderate gas pressures (∼10 bar).

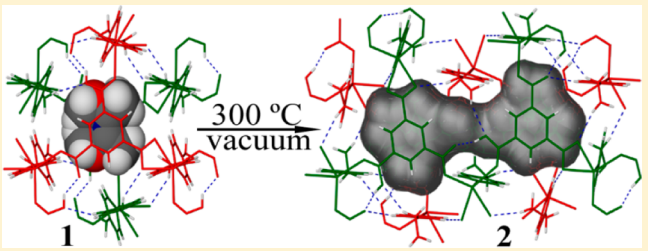

INTRODUCTION

Metal−organic frameworks (MOFs) have extended structures and typically contain either single or polynuclear metal centers interconnected by bridging organic ligands into one-, two-, or three-dimensional (1D, 2D, or 3D) networks. Owing to their high specific surface areas, tunable structures and functionalities, uniform pore size, and high degree of porosity, they have emerged as a promising class of materials for gas storage and separation, particularly for hydrogen, methane, and carbon dioxide.[1] As a building block to construct MOFs, 1,3,5-benzenetricarboxylic acid (H_3BTC) ligand exhibits a variety of coordination modes and has the capability of generating coordination architectures of diverse size and shape. There have been many reports on infinite 1D, 2D, and 3D coordination polymers using H_3BTC as a starting material in various states of deprotonation.[2] MOFs constructed by mixed ligands of pyridyl groups and carboxylate groups not only incorporate interesting properties of different functional groups but also lend themselves to a great variety of structures. The recent upsurge of interest in these materials is due to the robustness of MOFs with mixed ligands on loss of included solvent molecules. The high degree of porosity within MOFs can provide the necessary space to take up gas molecules, while the tunable pore sizes/curvatures and functionalized pore surfaces can be utilized to direct strong interactions with gas molecules.[3] Single-crystal-to-single-crystal (SC−SC) transformations in MOFs have attracted considerable attention as an interesting solid-state phenomenon[4] and are usually induced by various stimuli such as heat,[5] light,[6] solvent molecules,[7] or redox reagents.[8] Kitagawa and co-workers described a series of highly flexible MOFs using tris(2-carboxyethyl)isocyanurate (tci), which included $\{[Ce(tci)(H_2O)_2]\cdot 2H_2O\}_n$, $\{[Pr(tci)(H_2O)_2]\cdot 2H_2O\}_n$, and $\{[Cu_2(tci)(OH)(H_2O)_3]\cdot 1.5H_2O\}_n$ that exhibited reversible SC−SC transformation from 2D to 3D frameworks via thermal dehydration/rehydration processes[9] which involve cleavage and generation of coordination bonds. Perles et al. reported Sc(III)-

Received: November 30, 2012
Revised: February 22, 2013
Published: February 25, 2013

   dx.doi.org/10.1021/cg301760a | *Cryst. Growth Des.* 2013, 13, 1526−1534

Table 1. Crystal Data and Structure Refinement for 1, 2, and 3

	1	2	3
empirical formula	$C_{24}H_{23}Cd_1N_3O_7$	$C_{21}H_{16}CdN_2O_6$	$C_{21}H_{16}CdN_2O_6$
formula weight	577.85	504.77	504.77
temperature (K)	173(2)	173(2)	173(2)
λ (Å)	0.71073	0.71073	0.71073
crystal system	orthorhombic	orthorhombic	orthorhombic
space group	*Pbcm*	*Pbca*	*Pbcm*
unit cell dimensions (Å)	a = 10.4621(10)	a = 16.811(3)	a = 10.3913(8)
	b = 16.6080(15)	b = 13.891(3)	b = 16.7981(13)
	c = 13.9436(13)	c = 20.743(4)	c = 13.8612(11)
volume (Å^3)	2422.8(4)	4843.9(17)	2419.5(3)
Z	4	8	4
calc density (g cm^{-3})	1.587	1.387	1.386
μ(mm^{-1})	0.951	0.936	0.937
F_{000}	1172	2024	1008
crystal size (mm^3)	0.20 × 0.15 × 0.10	0.21 × 0.18 × 0.14	0.20 × 0.15 × 0.10
θ range for data collection (°)	1.95−25.00	2.83−25.00	1.96−24.99
Miller index ranges	$-12 \le h \le 8$, $-19 \le k \le 11$, $-16 \le l \le 16$	$-19 \le h \le 19$, $-16 \le k \le 16$, $-24 \le l \le 24$	$-12 \le h \le 11$, $-19 \le k \le 19$, $-16 \le l \le 16$
reflections collected	10409	77879	9491
independent reflections	2224 [R_{int} = 0.0516]	4255 [R_{int} = 0.0622]	2204 [R_{int} = 0.0298]
completeness to θ_{max} (%)	99.3	99.7	98.6
max and min transmission	0.91 and 0.83	0.88 and 0.83	0.91 and 0.84
refinement method	full-matrix least-squares on F^2	full-matrix least-squares on F^2	full-matrix least-squares on F^2
data/restraints/parameters	2224/7/238	4255/0/272	2204/18/211
goodness-of-fit on F^2	1.255	1.042	1.129
final R indices [$I > 2\sigma(I)$]	R_1 = 0.0510, wR_2 = 0.1557	R_1 = 0.0300, wR_2 = 0.0745	R_1 = 0.0499, wR_2 = 0.1283
R indices (all data)	R_1 = 0.0651, wR_2 = 0.1639	R_1 = 0.0437, wR_2 = 0.0808	R_1 = 0.0601, wR_2 = 0.1344
largest diff peak and hole (e Å^{-3})	1.089 and −0.877	1.076 and −0.459	1.160 and −0.884

based MOFs $\{[Sc_2(OH)(O_2CC_2H_4CO_2)_{2.5}]\}_n$, $\{[Sc_2(1,5\text{-}O_3SC_{10}H_6SO_3)(OH)_4]\}_n$, and $\{[Sc_2(2,6\text{-}O_3SC_{10}H_6SO_3)(OH)_4]\}_n$ with exceptional thermal stability up to 350−500 °C but did not show any SC−SC transformation.[10] Song et al. reported[11] the first SC−SC transformation observed in 4f-based MOFs, namely, the dehydration of $[Dy_2(phen)_2(L)_6]\cdot 2H_2O$ to anhydrous phase $[Dy_2(phen)_2(L)_6]$ (where L is β-naphthoic acid and phen is phenanthroline) by calcinations under a vacuum at 160 °C for 24 h. Bernini et al. showed[12] a reversible temperature induced SC−SC transformation in $[Yb(C_4H_4O_4)_{1.5}]$ which occurred at 130 °C. Cao et al. reported the MOFs $[M(OBPT)_2]\cdot 0.6H_2O$ (where OBPT = 4,6-bis(4-pyridyl)-1,3,5-triazin-2-ol and M = Co, Ni) which exhibits reversible SC−SC transformation driven by thermal treatment involving dehydration and rehydration processes.[13] Xue et al. reported[14] $[Cd(\mu\text{-}OH_2)(bct)]$ (where bct is bis(carboxymethylmercapto)-1,3,4-thiadiazole acid) to exhibit SC−SC transformation upon heating at 180 °C under a vacuum into dehydrated [Cd(bct)].

Previous work on the reaction between Cd(II) and H_3BTC has yielded a number of MOF structures based on either H_3BTC or mixed ligand systems, with the majority of these formed under hydrothermal conditions. Paz et al. reported[15] hydrothermal reaction between $Cd(NO_3)_2$, trimesic acid (H_3BTC), and 1,2-bis(4-pyridyl)ethane (BPE) in the presence of triethylamine to yield $[Cd_{1.5}(BTC)(BPE)(H_2O)_2]\cdot(H_2O)$. The authors reported that the absence of the base triethylamine instead yielded layered structures. Herein we report that when we used the same starting materials with a binary water and *N*,*N*′-dimethylformamide (DMF) solvent system, and in the absence of triethylamine, a porous, 3D MOF $[Cd(HBTC)\text{-}BPE]_n\cdot n$DMF was synthesized. The synthesized MOF exhibits SC−SC transformation upon desolvation and subsequent sorption of liquid and gaseous solvent molecules. Liquid sorption selectivity was toward nonpolar solvents such as benzene, toluene, THF, $CHCl_3$, and 1,4-dioxane, while gas sorption selectivity favored CO_2, N_2, and N_2O over H_2.

EXPERIMENTAL SECTION

Materials and Physical Measurements. All chemicals were of reagent grade, purchased from commercial sources, and used without further purification.

Elemental analysis was performed on a Thermo Flash EA-1112 CHNS-O elemental analyzer. The IR spectra were obtained from KBr pellets in the range 4000−400 cm^{-1}, using a Perkin-Elmer Spectrum 100 FT-IR spectrometer.

Hot-stage microscopy was performed on a Nikon SMZ-10 stereoscopic microscope fitted with a Linkam THMS600 hot stage and a Linkam TP92 control unit. Samples were placed under silicone oil on a coverslip and heated at 10 °C min^{-1}. Thermal events were monitored with a Sony Digital Hyper HAD color video camera and captured using the Soft Imaging System program analysis.[16]

Thermogravimetric (TG)/differential thermogravimetric (DTG) measurements were performed at a heating rate of 10 °C min^{-1} in the temperature range 25−600 °C, under a dry nitrogen flow of 60 mL min^{-1} on a TGA Q500 instrument. Approximately 2−5 mg of sample was placed in an open aluminum crucible.

Differential scanning calorimetry (DSC) measurements were performed at a heating rate of 10 °C min^{-1} in the temperature range 25−400 °C, under a dry nitrogen flow of 50 mL min^{-1} on a DSC Q200 instrument. Approximately 1−2 mg of sample was placed in an aluminum pan with a lid. A sealed and empty pan was used as a reference.

dx.doi.org/10.1021/cg301760a | *Cryst. Growth Des.* 2013, 13, 1526−1534

Powder X-ray diffraction (XRD) analysis was performed on a HUBER-Guinier 670 Imaging Plate X-ray powder diffractometer using Cu Kα radiation (λ = 1.5405 Å) generated by a Philips X-ray generator at 40 kV and 20 mA. A sample was placed in a 1 mm capillary tube, and a diffraction pattern was acquired under ambient conditions in transmission mode while the sample rotation axis was perpendicular to the beam.

Synthesis of 1. Trimesic acid (20 mg, 0.095 mM) and 1,2-bis(4-pyridyl)ethane (18 mg, 0.095 mM) were dissolved in 4.8 mL of DMF, whereas $Cd(NO_3)_2{\cdot}4H_2O$ (29 mg, 0.095 mM) was dissolved in 3.6 mL of H_2O and acidified with H_2SO_4 (1 M, 0.2 mL). Both the solutions were heated, and hot clear solutions were combined in a sealed vial and kept in a Dewar flask. The solution was slowly cooled in the Dewar flask from 80 °C to room temperature over a period of 2 days, which yielded good quality colorless crystals (17 mg, 35%). Anal. Calc: for $C_{24}H_{24}N_3O_7Cd_1$ (FW = 578.88): C, 49.75; H, 4.14; N, 7.25. Found: C, 49.48; H, 4.00; N, 7.45. IR (KBr, cm^{-1}): 3361, 2936, 1612, 1576, 1504, 1434, 1369, 1224, 1072, 1016, 831, 756, 691, 548, 487.

Synthesis of 2. Heating the colorless crystals of **1** at 300 °C for 5 h in an oven under a vacuum results in the formation of **2**. The crystals were stable and only the solvent was removed.

Synthesis of 3, 4, and 5. Crystals of **2** were soaked in benzene (**3**), chloroform (**4**), and THF (**5**) and checked for their respective unit cells. It was observed that the unit cell values were similar to solvated **1**. Data were collected for **3**, **4**, and **5**, but only in the case of **3** could the host framework be satisfactorily refined. In all cases, the guest molecules were too disordered to be assigned despite their presence being confirmed by TG results.

Single Crystal X-ray Diffraction Analysis and Structure Determination. Suitable single crystals of **1**, **2**, **3**, **4**, and **5** were selected and coated with oil before being mounted in air onto a loop. The data collection for **1** and **3**, **4**, and **5** was carried out with a Bruker DUO APEX II CCD diffractometer at 173(2) K using an Oxford Cryostream-700. Data reduction and cell refinement were performed using SAINT-Plus,[17] and the space group was determined from systematic absences by XPREP[18] and confirmed using the program Layer.[19]

The data collection for **2** was carried out with a Nonius Kappa CCD diffractometer at 173(2) K using an Oxford Cryostream-600. Data reduction and cell refinement were performed using DENZO,[20] and the space group was determined from systematic absences by XPREP.[18]

Graphite monochromated Mo Kα (λ = 0.71073 Å) radiation was used in both cases. The X-ray diffraction data have been corrected for Lorentz-polarization factor and scaled for absorption effects by multiscan using SADABS.[21] The structures were solved by direct methods, implemented in SHELXS-97.[22] Refinement procedure by full-matrix least-squares methods based on F^2 values against all reflections have been performed by SHELXL-97,[22] including anisotropic displacement parameters for all non-H atoms.

Calculations concerning the molecular geometry, the affirmation of chosen space groups, and the analysis of hydrogen bonds were performed with PLATON.[23] The molecular graphics were rendered with ORTEP-3[24] and MERCURY (Version 3.0).[25] The calculated PXRD patterns of **1**, **2**, and **3** were generated by Lazy Pulverix.[26] The crystal parameters, data collection, and refinement results for **1**–**3** are summarized in Table 1.

CCDC 908241–908243 contain the supplementary crystallographic data for this paper. These data can be obtained free of charge via www.ccdc.cam.ac.uk/data_request/cif [or from the Cambridge Crystallographic Data Centre (CCDC), 12 Union Road, Cambridge CB2 1EZ, U.K.; fax: +44(0)1223-336033; e-mail: deposit@ccdc.cam.ac.uk].

Gas Sorption Analysis. The procedure in the gas sorption analysis was followed according to the method described by Atwood et al.[27] The apparatus consisted of two chambers A and B, which were connected to pressure sensors P_a and P_b. The chambers were connected to a gas line, while the gas-flow into and between the chambers was regulated by two valves. Chamber A is left empty as a control, while chamber B contains the sample of known mass, and the whole system was evacuated under heat (65 °C, maximum of the equipment) in order to remove any residual solvent. After the system was cooled down to 25 °C, approximately 20 bar of pressure was released from the gas cylinder into chamber A. The valve between the chambers was then opened and closed rapidly, allowing a certain amount of gas into chamber B (volumes of both A and B were known). The pressure in chamber A remained constant, and any decrease in the pressure in chamber B indicated that gas was being sorbed by the sample. Gas pressures in chambers A and B were monitored using the program *Absorbance*.[28] From the measurement of the decrease in pressure over time, the percentage sorption by mass of the material was calculated.

RESULTS AND DISCUSSION

The reaction between $Cd(NO_3)_2{\cdot}4H_2O$, trimesic acid (H_3BTC), and 1,2-bis(4-pyridyl)ethane (BPE) gives rise to a highly crystalline product formulated as $[Cd(HBTC)\text{-}BPE]_n{\cdot}nDMF$ (**1**) (Scheme 1), in which infinite 2D sheets pillared by flexible bipyridyl ligands to form a 3D framework. Interestingly, heating the single crystals of **1** at 300 °C for 5 h under a vacuum resulted in a SC–SC transformation of **1** into the desolvated form **2** formulated as $[Cd(HBTC)BPE]_n$ with double the unit cell volume of **1**.

Scheme 1. Synthesis of 1

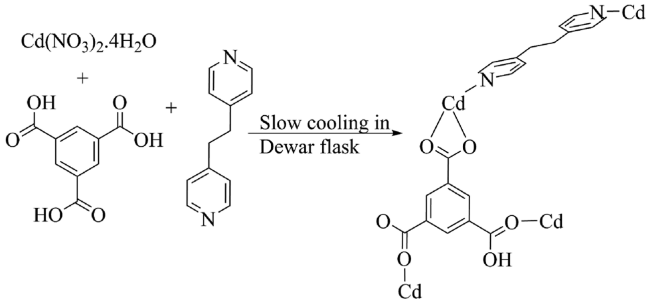

Structure of 1. X-ray single-crystal analysis reveals that the structure contains a distinct repeating structural motif containing a unique Cd^{2+} cation in a distorted octahedral coordination geometry (Figure 1). Crystallographic data, selected bond lengths and bond angles are listed in Tables 1, 2, and S1. The asymmetric unit of **1** consists of 0.5 units of Cd(II), $HBTC^{2-}$, BPE, and DMF. Cd(1) is coordinated to four oxygen donor atoms from three $HBTC^{2-}$ anions in the equatorial plane and to two nitrogen donor atoms from two 1,2-bis-(4-pyridyl)ethane ligands occupying the apical positions (Figure 1). The Cd–O and Cd–N bond distances are 2.331 Å (average) and 2.319(6) Å (Tables 2 and S1) respectively. Each trimesate anion bridges three metal centers through its three functional groups in two different coordination modes (Scheme 1 and Figure 1) to form 2D parallelogram-like sheets $[Cd(HBTC)]_n$ parallel to the *ab* plane. Adjacent sheets are connected by BPE ligands to form a 3D layered framework. The first carboxylate group (C1/O1/O2) is bonded to Cd^{2+} in a symmetrical bidentate chelating mode with the angle subtended at the metal atom being 55.5(2)°, while the two carboxylic acid groups bond via the carbonyl oxygen atoms (O3 and O5) in a monodentate fashion (Scheme 1). The carboxylate and carboxylic acid groups are coplanar with respect to the phenyl ring. The Cd---Cd distances across the parallelogram-like sheets $[Cd(HBTC)]_n$ are 10.462 and 9.364 Å along the *a*- and *b*-axes, respectively.

The bidentate BPE ligands bridge translated metal centers along the [001] direction, thus connecting adjacent [Cd-

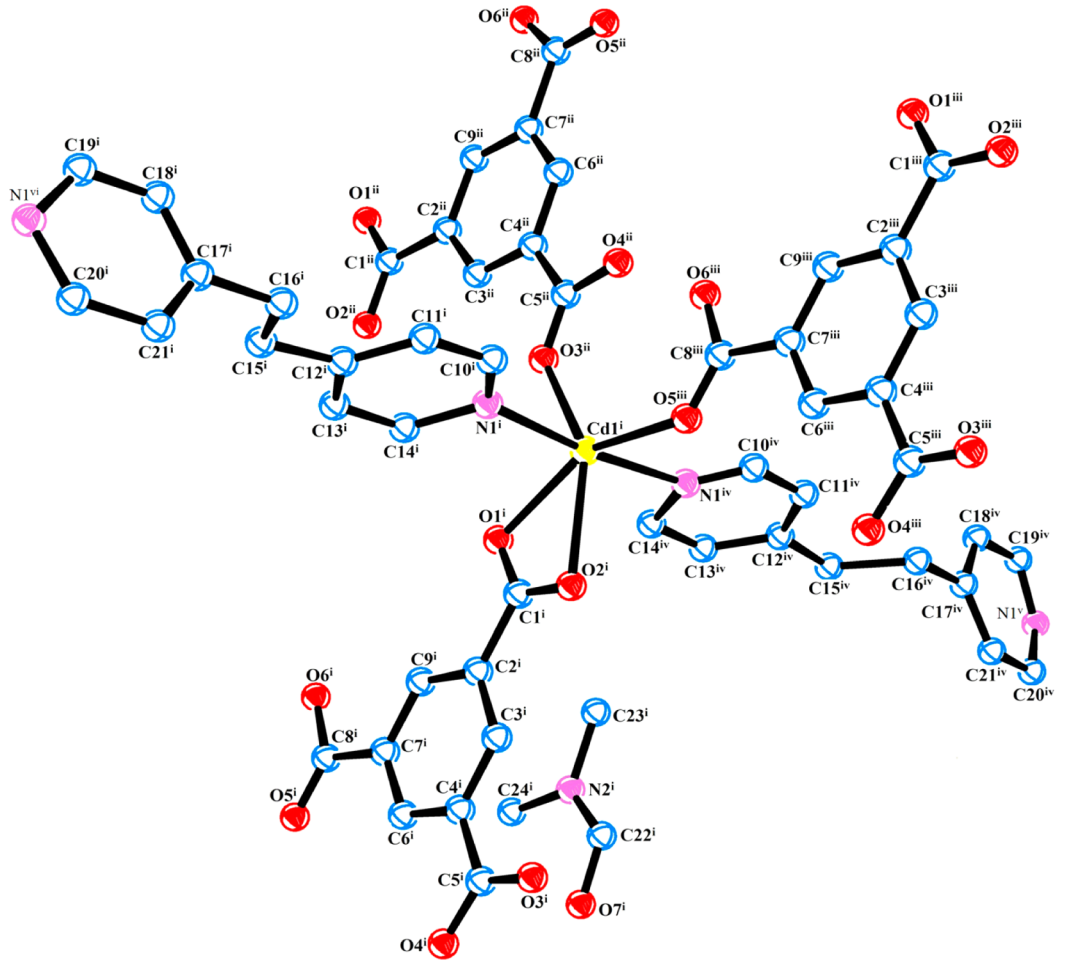

Figure 1. ORTEP plot of **1** showing the coordination environment of Cd(II) (thermal ellipsoids are drawn at the 30% probability level). Disordered atoms and hydrogen atoms have been omitted for clarity. Symmetry equivalent positions are (i) x, y, z; (ii) $1 - x, 1/2 + y, 1/2 - z$; (iii) $1 + x, y, z$; (iv) $x, y, 1/2 - z$; (v) $x, y, z - 1$; (vi) $x, y, 3/2 - z$.

$(HBTC)]_n$ layers to afford a 3D open framework (Figure 2). The BPE ligand adopts an anticonformation ($C-CH_2-CH_2-C$ torsion angle of 180°); however, the pyridyl rings are nearly perpendicular to each other (interplanar angle being 72.48°). The Cd---Cd separation across the BPE ligand is 13.863 Å. It may be regarded as a pillar of the $[Cd(HBTC)]_n$ layers through *trans*-coordination.

The non-nitrogen atoms of the BPE ligands are disordered over two positions with site occupancy factors of 50% as required by a crystallographic mirror plane across which the molecule is located (the mirror plane is perpendicular to the long axis of the molecule). The DMF molecule is uncoordinated and disordered over two positions with site occupancy factors of 50%. All bond distances of the DMF molecule were restrained to ideal values as unrestrained refinement lead to unacceptable bond distances and angles. A 2-fold rotation axis ($x, 1/2 - y, -z$) with direction [100] at [x, 1/4, 0] passes through the center of the DMF molecule which relates one disordered position to the other. The structural analysis revealed the $[Cd(HBTC)]_n$ layers are positioned on mirror planes perpendicular to [001]. The cadmium and the trimesate ligand act as 3-connecting linkers in the *ab*-plane, so overall adopts a 2D sheet structure which further extends in the third dimension via the Cd^{2+} ions using BPE linkers as shown in Figure 2. The structure comprises a 2-fold interpenetrated network with cavities containing one DMF molecule each (Figure 2). A short, strong hydrogen bond reinforces the monodentate coordination mode of the two carboxylic groups [O(4)···O(6) 2.389(14) Å, H(4a)···O(6) 1.69 Å, O(4)–H(4a)···O(6) 139°, ($-x, 1/2 + y, -1/2 - z$)] forming an eight-membered ring involving Cd1. The interpenetrated frameworks interact through C–H···O interactions [C(15)···O(1) 3.29(2) Å, H(15B)···O(1) 2.46 Å, C(15)–H(15B)···O(1) 141°, ($1 - x, -y, 1/2 + z$)] and [C(16)···O(4) 3.395(18) Å, H(16B)···O(4) 2.43 Å, C(16)–H(16B)···O(4) 164°, ($1 + x, 1/2 - y, -z$)] (Figure 4a) between the BPE ethylene hydrogen atoms and the oxygen atoms of the $HBTC^{2-}$ anions, respectively.

Structure of 2. When single crystals of **1** were heated at 300 °C under a vacuum for 5 h, SC–SC transformation of **1** into the desolvated form **2** was observed. Structure elucidation by single crystal X-ray diffraction of **2** confirms that the framework structure and packing mode of **1** are retained and that the space previously occupied by DMF molecules becomes devoid of any appreciable electron density (Figure S1 and Figure 3). This was further confirmed by TG analysis with no appreciable mass loss occurring for **2** over the temperature range of 25–300 °C. Crystallographic data, selected bond lengths, and bond angles are listed in Tables 1, 2, and S1. The transformation from **1** to **2** involves changes in space group symmetry (from *Pbcm* to *Pbca*) but in effect amounts to similar lattice parameters (although axis ~10 Å doubles to ~20 Å) and

dx.doi.org/10.1021/cg301760a | *Cryst. Growth Des.* 2013, 13, 1526–1534

Table 2. Bond Lengths [Å] for 1, 2, and 3

(1)		(2)		(3)	
Cd(1)–O(1)	2.297(6)	N(1)–Cd(1)	2.290(3)	Cd(1)–O(1)	2.391(5)
Cd(1)–O(3)#1	2.298(7)	N(2)–Cd(1)#2	2.294(3)	Cd(1)–O(2)	2.346(6)
Cd(1)–O(5)#2	2.315(6)	O(1)–Cd(1)	2.265(2)	Cd(1)–O(4)#1	2.289(7)
Cd(1)–N(1)	2.319(7)	O(3)–Cd(1)#1	2.364(2)	Cd(1)–O(6)#4	2.374(6)
Cd(1)–O(2)	2.417(6)	O(4)–Cd(1)#1	2.384(2)	Cd(1)–N(10)	2.293(5)
O(1)–C(1)	1.258(10)	O(5)–Cd(1)#3	2.400(2)	O(1)–C(1)	1.255(9)
C(1)–O(2)	1.242(10)	C(1)–O(1)	1.247(4)	C(1)–O(2)	1.266(9)
O(3)–C(5)	1.201(10)	C(1)–O(2)	1.256(4)	O(3)–C(9)	1.283(15)
O(4)–C(5)	1.255(12)	C(8)–O(4)	1.252(4)	O(4)–C(9)	1.209(12)
O(5)–C(8)	1.196(10)	C(8)–O(3)	1.265(3)	O(5)–C(8)	1.288(12)
O(6)–C(8)	1.274(12)	C(9)–O(5)	1.217(4)	O(6)–C(8)	1.177(11)
		C(9)–O(6)	1.293(4)		

Symmetry transformations used to generate equivalent atoms:

#1 $-x+1, y+1/2, z$ #1 $x, -y+3/2, z-1/2$; #2 $x, y-1, z$ #1 $x+1, y, -z+1/2$

#2 $x+1, y, z$ #3 $x+1/2, -y+3/2, -z$ #4 $-x+2, y-1/2, z$

molecular stacking arrangements. Despite the close similarity in unit cell parameters of **1** and **2**, the structures are indeed different as unequivocally demonstrated by the diffraction data; i.e., it is not possible to index **1** with the same unit cell as **2**.

The asymmetric unit of **2** consists of one Cd(II), one $HBTC^{2-}$ anion, and one BPE molecule. The coordination environment of Cd(1) and the connectivity are the same as in the parent molecule (Figure 1). The average Cd–O bond distance of 2.354 Å is longer than the parent molecule (2.331 Å), while the Cd–N bond distance of 2.292 Å is smaller than that of the parent molecule (2.319 Å) (Table 2 and S1). The carboxylate groups deviate slightly from the plane of the corresponding linking phenyl ring. The Cd---Cd separation across the parallelogram-like sheets $[Cd(HBTC)]_n$ being 10.379 (10.462 Å in **1**) and 9.386 Å (9.364 Å in **1**) along the *c*- and *a*-axis, respectively. As in the case of **1**, strong hydrogen bonds reinforce the monodentate coordination mode of the carboxylic group [O(2)–H(2)---O(6)] forming an eight-membered ring each involving Cd1 (Table 3).

The following description of the network topology of **2** is applicable to that of **1** as well (crystallographic axes labels are different in **1** and **2**). Each Cd(II) center serves as a 5-connected node by linking to three $HBTC^{2-}$ anions with the vertex symbol of $(6.6.6.6_2.6_2.6_2.6_2.6_2.6_2.8_6)$, and each $HBTC^{2-}$ anion represents a 3-connected node by linking to three Cd(II) with the vertex symbol of $(6_3.6_3.6_3)$ to generate sheets parallel to the *ac*-plane, which in turn are connected in the third dimension by BPE ligands. The sheets feature a honeycomb-like layer with topological representation of 6^3. Thus, a 3-D (3,5)-connected network with the Schläfli symbol of $\{\hat{6}3\}\{\hat{6}9.8\}$-VS[6.6.6.6(2).6(2).6(2).6(2).6(2).6(2).*]-

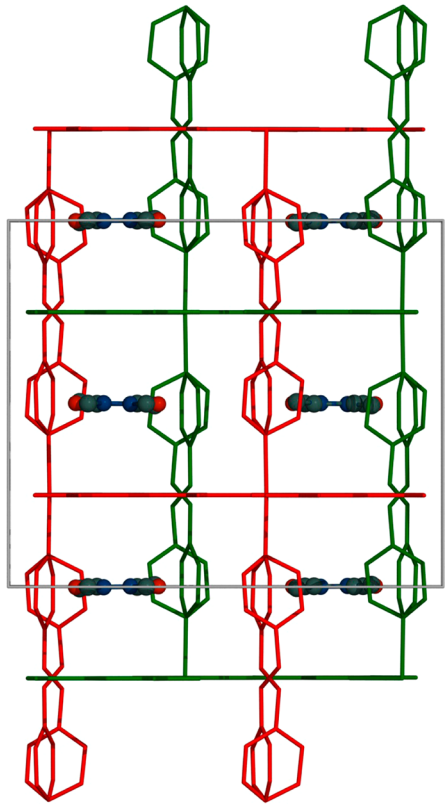

Figure 2. View down the *a*-axis showing the 2-fold interpenetrated pillared network (individual frameworks are depicted in red and green respectively) of **1**.

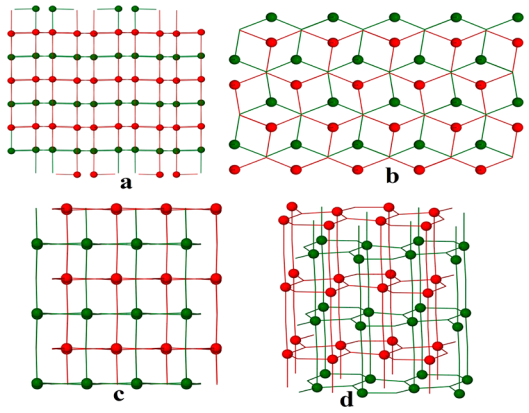

Figure 3. Views of the 2-fold-interpenetrated 3D topological network for **2** constructed from two identical hexagonal nets viewed down the (a) *a*-axis, (b) *b*-axis, (c) *c*-axis. (d) *hms* topology network displaying hexagonal packing.

[6(3).6(3).6(3)] is generated with doubly interpenetrated (3,5)-connected *hms* topology[29] as depicted in Figure 3. As in the case of **1**, the interpenetrated frameworks interact through C–H---O interactions (Figure 4b) between the ethylene H15b and H16b to O3 and O6 and phenyl C–H (H18 and H21) to O4 and O2 of carboxylic groups, respectively, which may be responsible for the structural stability of **2**.

Two-fold interpenetration leads to the disappearance of the big channels of the individual frameworks, and to the subsequent formation of small cavities formed by the $HBTC^{2-}$ anion and BPE ligands of both frameworks. In **1**

dx.doi.org/10.1021/cg301760a | *Cryst. Growth Des.* 2013, 13, 1526–1534

Table 3. Hydrogen Bonds in Compound 2

donor---H····acceptor	symmetry equivalent positions	H····A	D····A	D−H····A
O(2)−H(2)····O(6)	[1/2 + *x*, 1/2 − *y*, −*z*]	2.15	2.468	103
C(15)−H(15B)····O(3)	[1 − *x*, −*y*, −*z*]	2.36	3.3145	161
C(16)−H(16B)····O(6)	[1/2 − *x*, −1/2 + *y*, *z*]	2.47	3.3639	150
C(18)−H(18)····O(4)	[1/2 − *x*, −*y*, 1/2 + *z*]	2.58	3.4723	156
C(21)−H(21)····O(2)	[1 − *x*, −*y*, −*z*]	2.59	3.5217	166

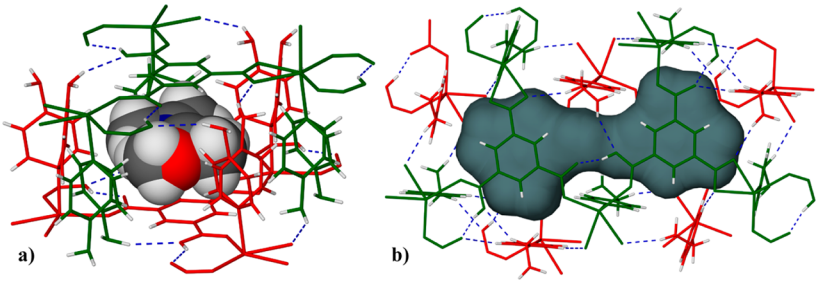

Figure 4. (a) A DMF molecule (displayed in space-filling mode) situated in a cavity of **1**. Non-nitrogen atoms of the pyridyl rings are disordered over two positions with site occupancy factors of 50%. (b) Cavity formed in **2** by the evacuation of DMF in **1**. Two-fold interpenetrated networks (3,5-connected *hms* topology) are shown in red and green for both **1** and **2**, and C−H···O and O−H···O interactions between the frameworks are shown for **2** (also present in **1**).

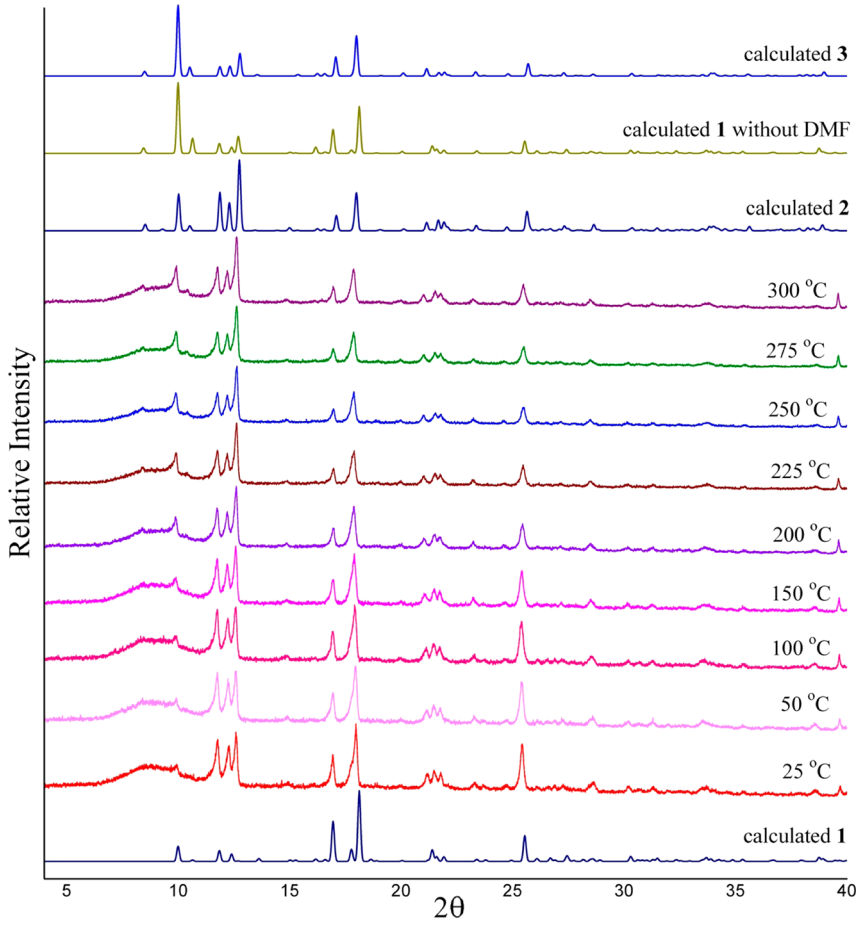

Figure 5. PXRD pattern at variable temperature and compared with the calculated patterns of **1**, **2**, and **3**.

these cavities are isolated, have a size of 158 Å^3, and are occupied by a single DMF molecule (Figure 4a). The desolvation of **1** upon heating must thus involve cooperative conformational changes in the frameworks in order to allow for the evacuation of the DMF molecules with the retention of monocrystallinity. Interestingly, in **2** the cavity size effectively doubles to 328 Å^3 (Figure 4b) as a result of two neighboring pyridyl groups from different frameworks which "opens" and allows two neighboring cavities to "connect" as when compared to **1**. The disorder in structure **1** prohibits this scenario of two

dx.doi.org/10.1021/cg301760a | *Cryst. Growth Des.* 2013, 13, 1526−1534

parallel pyridyl rings as the other disordered component (as required by the mirror plane in **1**) will put the neighboring pyridyl groups in too close a proximity. This illustrates that neighboring pyridyl rings in **2** are rotated differently with respect to one another when compared to both disordered situations in **1**, which further supports that the frameworks of **1** and **2** indeed have subtle differences, aiding our argument that the desolvation process may be described as a SC−SC transformation.[30] The total potential solvent area volumes of 1311 Å^3 represent 27.1% of the unit cell volume for structure **2** (volumes were determined using PLATON with 1.2 Å probe radius).[23]

Structure of 3. When single crystals of **2** were soaked in benzene overnight, SC−SC transformation of **2** to solvated compound **3** (**2·benzene**) was observed. Single crystal X-ray diffraction of **3** confirms that the framework structure and packing mode are retained but the unit cell values are similar to **1**. Crystallographic data, selected bond lengths, and bond angles are listed in Tables 1, 2, and S1.

Due to disorder within the structure, we were only able to observe some electron density within the pores of **3** by single crystal X-ray diffraction but were not able to assign specific atom positions for the benzene molecule,[31] despite the presence of the benzene molecule (1:1 ratio) being confirmed by TG.

Single Crystal−Single Crystal Transformation Triggered by Thermal Treatment. PXRD was used to check the structural identity and possible phase transition of **1** into **2**. Due to the close similarity of the crystal structures of **1** and **2**, it is not surprising that their calculated powder patterns are virtually identical. However significant differences do exist as illustrated in Figure 5.

The room temperature PXRD pattern of **1** closely resembles that of the calculated pattern; however the three peaks at 11−13° 2θ resemble that of the calculated pattern of **2**, which perhaps indicates that some of the sample may already have desolvated when the analysis commenced. Despite repeated attempts, we could not obtain an experimental pattern of different samples of **1** which resembles that of the calculated PXRD pattern more closely. We do however observe a general trend of the experimental PXRD pattern of **1** to resemble that of the calculated pattern of **2** with increasing temperature. For example, the shoulder at 2θ = 17° starts disappearing, the peaks at 2θ = 10−13° increase in relative intensity to the peak at 2θ = 17°, while the peaks at 2θ = 25.6−27.5° separate. More importantly, PXRD measurements at variable temperatures illustrated the robustness of the framework upon removal of DMF molecules and up to 300 °C. The patterns calculated from the crystal structure of **3** and calculated from that of **1** (DMF coordinates omitted) are also included in Figure 5 for reference.

TGA. The TGA data of complex **1** indicate two mass losses (Figure S2). The first mass loss 115−350 °C (13.2%) corresponds to the loss of half a DMF molecule per asymmetric unit (calculated: 12.6%). An abrupt mass loss in the range 360−480 °C (66.2%) corresponds to structure decomposition. DSC shows only one broad endotherm peak which should be due to the loss of DMF (Figure S2). Hot stage microscopy indicates that visual loss of DMF occurs for **1** in the temperature range 270−280 °C (Figure 6). Visual observation of chloroform and benzene release (Figure 6) was also recorded for the crystals of **3** and **4**, respectively, under the hot stage microscope by immersing the sample in silicone oil and heating to 300 °C.

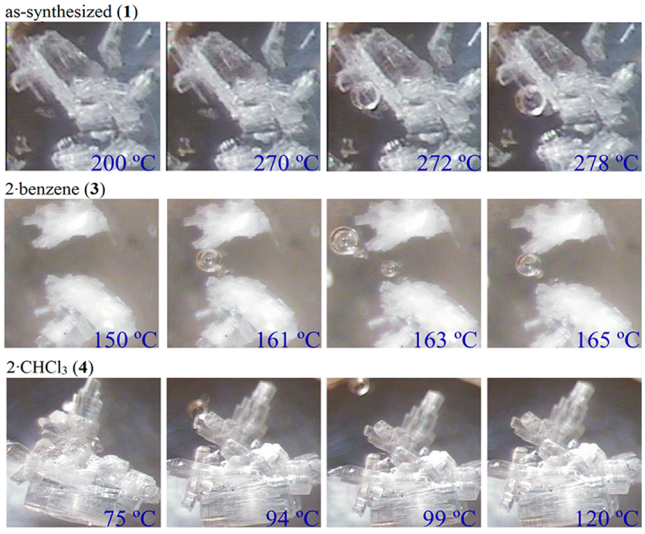

Figure 6. Hot stage microscope photographs of compounds **1**, **2·benzene** (**3**), and **2·CHCl$_3$** (**4**) showing the release of solvents at various temperatures.

Bubbles of chloroform and benzene were released in the range 90−110 °C and 160−170 °C, respectively. The TGA analysis for **3**, however, revealed a clear mass loss (12.3%) between 160−170 °C (Figure S3).

Sorption of Organic Solvents. Due to the great stability of framework the uptake of different solvent molecules was analyzed. Therefore few crystals of **2** were immersed into the different solvents (DMF, ethanol, methanol, mesitylene, THF, C_6H_6, $CHCl_3$, CH_2Cl_2, toluene, and 1,4-dioxane) overnight and afterward thermogravimetric analyses were performed (Figure S3 and Table 3). Compound **2**·solvent showed a prolonged weight loss in the range of 60−250 °C for benzene, 30−250 °C for $CHCl_3$, 30−100 °C THF and 30−215 °C for 1,4-dioxane that amounted to 11.63, 16.18, 12.34, and 16.79%, respectively (Table 4). The different profiles of the TGA suggest that the uptakes were not simply due to different amounts of water absorbed in the event that the solvents used were wet.

Table 4. Results of the Solvent Uptake Experiment

entry	**2**·solvent	% mass loss in TGA	% calculated mass loss[a]
1	DMF	3.02	12.6
2	EtOH	0.1	8.3
3	MeOH	0.6	5.9
4	mesitylene	2.5	19.2
5	benzene	11.63	13.3
6	chloroform	16.18	19.1
7	toluene	6.86	15.4
8	DCM	10.44	14.3
9	1,4-dioxane	16.79	14.8
10	THF	12.34	12.4

[a]Calculated % mass loss for the case that every cavity is occupied by one solvent molecule.

As shown in Table 4 there was a high selectivity for the benzene, chloroform, 1,4-dioxane, and THF, whereas it was not possible to resorb the DMF again to the same degree as for these solvents. Due to the higher affinity of the compound to some solvents than to DMF, it was assumed that a guest exchange might also be possible. Hence some crystals of the as-

dx.doi.org/10.1021/cg301760a | Cryst. Growth Des. 2013, 13, 1526−1534

synthesized, DMF containing compound **1** were immersed in chloroform, H_2O, ethanol, methanol, benzene, dichloromethane, tetrahydrofuran, and 1,4-dioxane for overnight and analyzed by TGA afterward. However, the TGA spectrum only showed a mass loss (the same value as original) at the temperature range of 200−300 °C which is specific for the loss of the DMF and not for other solvents, which should occur at lower temperature. It was assumed that there was no guest exchange between the two solvents, which is remarkable because the structure seems to be having a higher affinity for nonpolar solvents than for DMF. This could be due to slight conformational difference in **1** and **2** change which allows passage of molecules in **2** whereas the release of DMF molecules in **1** requires heating to higher temperatures. In all cases, the sorption of the various organic solvents seemed to be SC−SC transformations as judged from visual observations as well as the ability to in each case determine unit cells using single crystal X-ray diffraction.

Gas Sorption. Due to the high total potential solvent area of 1311 Å^3 per unit cell volume or 27.1% for **2** gas sorption experiments were performed. The structure showed comparable sorption of 2.5% N_2, 4.5% CO_2 and 3.4% N_2O absorption by mass at a pressure of 9−12 bar. The graphs of the gas sorption are shown in Figure 7, the sorption of N_2, CO_2, and N_2O occur rapidly within the first few minutes of the analysis. Hydrogen sorption by **2** was negligible.

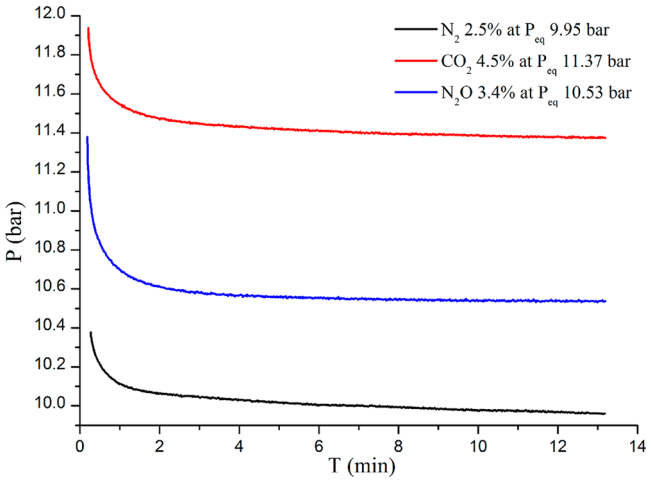

Figure 7. Gas sorption in **2** (N_2: black; N_2O: blue; CO_2: red).

IR. The strong asymmetric (ν_{as}) and symmetric vibrations (ν_s) of the carboxylate groups are located at 1612, 1578, 1434, and 1369 cm^{-1} (Figure S4). The differences between ν_{as} and ν_s of 144 cm^{-1} and 243 cm^{-1} indicate bidentate and unidentate coordination mode of carboxylate group, which is also confirmed by single-crystal structure determinations.[32] There is a shoulder peak at 1673 cm^{-1}, which indicates that there is protonated carboxyl group in the complex. Compared with the usual reports for protonated carboxyl group at 1720−1680 cm^{-1}, this peak shifts to lower wavenumber due to H-bond interaction.[33] Weak and broad absorption at 1739 cm^{-1} corresponds to DMF. IR spectrum for desolvated **2** was also recorded and found to be the same except that of absorption at 1739 cm^{-1} which disappears.

CONCLUSION

In conclusion, a new 3D MOF has been synthesized based on $Cd(NO_3)_2$, trimesic acid, and 1,2-bis(4-pyridyl)ethane, which exhibits temperature-induced SC−SC transformation involving the release of DMF molecules. The resulting desolvated form is highly stable up to 350 °C and exhibits single-crystal-to-single-crystal transformation in selected solvents (benzene, chloroform, 1,4-dioxane, and THF molecules over other polar solvents). The desolvation and solvation processes must involve cooperative conformational changes in the structures in order to retain monocrystallinity. In addition, the solvated and desolvated states of the framework reveal structural differences which further supports describing the desolvation/solvation processes as SC−SC transformations. The solvent-free porous framework shows a total potential solvent area of 27.1% of the structures' volume. The structure showed 2.5% N_2, 4.5% CO_2, and 3.4% N_2O absorption by mass. Studies are underway in our laboratory to further explore the robustness of this MOF system and to explain the selectivity of the sorption of the investigated solvents and gases.

ASSOCIATED CONTENT

Supporting Information

Figures S1−S4, Table S1 and X-ray crystallographic information files (CIF) are available for compounds **1**−**3**. This material is available free of charge via the Internet at http://pubs.acs.org.

AUTHOR INFORMATION

Corresponding Author

*E-mail: Clive.Oliver@uct.ac.za.

Notes

The authors declare no competing financial interest.

ACKNOWLEDGMENTS

A.H. and C.L.O. thank the South African National Research Foundation and the University of Cape Town for financial support.

REFERENCES

(1) (a) Zhao, D.; Yuan, D.; Zhou, H.-C. *Energy Environ. Sci.* **2008**, *1*, 222−235. (b) Sculley, J.; Yuan, D.; Zhou, H.-C. *Energy Environ. Sci.* **2011**, *4*, 2721−2735. (c) Murray, L. J.; Dinca, M.; Long, J. R. *Chem. Soc. Rev.* **2009**, *38*, 1294−1314. (d) Hirscher, M. *Angew. Chem., Int. Ed.* **2011**, *50*, 581−582. (e) Ma, S.; Zhou, H.-C. *Chem. Commun.* **2010**, *46*, 44−53. (f) Zhou, W. *Chem. Rec.* **2010**, *10*, 200−204. (g) D'Alessandro, D. M.; Smit, B.; Long, J. R. *Angew. Chem., Int. Ed.* **2010**, *49*, 6058−6082. (h) Li, J.-R.; Kuppler, R. J.; Zhou, H.-C. *Chem. Soc. Rev.* **2009**, *38*, 1477−1504. (i) Li, J.-R.; Ma, Y.; McCarthy, M. C.; Sculley, J.; Yu, J.; Jeong, H.-K.; Balbuena, P. B.; Zhou, H.-C. *Coord. Chem. Rev.* **2011**, *255*, 1791−1823. (j) Lu, W.; Yuan, D.; Makal, T. A.; Li, J.-R.; Zhou, H.-C. *Angew. Chem., Int. Ed.* **2012**, *51*, 1580−1584.

(2) (a) Eddaoudi, M.; Li, H.; Yaghi, O. M. *J. Am. Chem. Soc.* **2000**, *122*, 1391−1397. (b) Yaghi, O. M.; Li, H.; Groy, T. L. *J. Am. Chem. Soc.* **1996**, *118*, 9096−9101. (c) Yaghi, O. M.; Davis, C. E.; Li, G.; Li, H. *J. Am. Chem. Soc.* **1997**, *119*, 2861−2868. (d) Fang, Q.; Zhu, G.; Xue, M.; Sun, J.; Sun, F.; Qiu, S. *Inorg. Chem.* **2006**, *45*, 3582−3587. (e) Yaghi, O. M.; Li, G.; Li, H. *Nature* **1995**, *378*, 703−706. (f) Eddaoudi, M.; Moler, D. B.; Li, H.; Chen, B.; Reineke, T. M.; O'Keeffe, M.; Yaghi, O. M. *Acc. Chem. Res.* **2001**, *34*, 319−330. (g) Chui, S. S.-Y.; Lo, S. M.-F.; Charmant, J. P. H.; Orpen, A. G.; Williams, I. D. *Science* **1999**, *283*, 1148−1150. (h) Plater, M. J.; Foreman, M. R. S. J.; Howie, R. A.; Skakle, J. M. S.; Coronado, E.; Gomez-Garcia, C. J.; Gelbrich, T.; Hursthouse, M. B. *Inorg. Chim. Acta* **2001**, *319*, 159−175. (i) Prior, T. J.; Rosseinsky, M. J. *Chem. Commun.*

2001, 1222−1223. (j) Sun, D.; Cao, R.; Weng, J.; Hong, M.; Liang, Y. *Dalton Trans.* **2002**, 291−292. (k) Dai, J.-C.; Wu, X.-T.; Fu, Z.-Y.; Cui, C.-P.; Hu, S.-M.; Du, W.-X.; Wu, L.-M.; Zhang, H.-H.; Sun, R.-Q. *Inorg. Chem.* **2002**, *41*, 1391−1396. (l) Wu, G.; Shi, X.; Fang, Q.; Tian, G.; Wang, L.; Zhu, G.; Addison, A. W.; Wei, Y.; Qiu, S. *Inorg. Chem. Commun.* **2003**, *6*, 402−404. (m) Zhu, H.-F.; Sun, W.-Y.; Okamura, T.-A.; Ueyama, N. *Inorg. Chem. Commun.* **2003**, *6*, 168−173. (n) Lu, Z.-L.; Chen, W.; Xu, J.-Q.; Zhang, L.-J.; Pan, C.-L.; Wang, T.-G. *Inorg. Chem. Commun.* **2003**, *6*, 244−248. (o) Chen, J.-X.; Liu, S.-X.; Gao, E.-Q. *Polyhedron* **2004**, *23*, 1877−1888.

(3) (a) Hong, D.-Y.; Hwang, Y. K.; Serre, C.; Ferey, G.; Chang, J.-S. *Adv. Funct. Mater.* **2009**, *19*, 1537−1552. (b) Perry, J. J.; Perman, J. A.; Zaworotko, M. J. *Chem. Soc. Rev.* **2009**, *38*, 1400−1417. (c) Lin, X.; Telepeni, I.; Blake, A. J.; Dailly, A.; Brown, C. M.; Simmons, J. M.; Zoppi, M.; Walker, G. S.; Thomas, K. M.; Mays, T. J.; Hubberstey, P.; Champness, N. R.; Schroder, M. *J. Am. Chem. Soc.* **2009**, *131*, 2159−2171. (d) Nelson, A. P.; Farha, O. K.; Mulfort, K. L.; Hupp, J. T. *J. Am. Chem. Soc.* **2009**, *131*, 458−460. (e) Furukawa, H.; Ko, N.; Go, Y. B.; Aratani, N.; Choi, S. B.; Choi, E.; Yazaydin, A. O.; Snurr, R. Q.; O'Keeffe, M.; Kim, J.; Yaghi, O. M. *Science* **2010**, *329*, 424−428. (f) Farha, O. K.; Spokoyny, A. M.; Hauser, B. G.; Bae, Y.-S.; Brown, S. E.; Snurr, R. Q.; Mirkin, C. A.; Hupp, J. T. *Chem. Mater.* **2009**, *21*, 3033−3035. (g) Lin, Z.-J.; Liu, T.-F.; Xu, B.; Han, L.-W.; Huang, Y.-B.; Cao, R. *Cryst. Eng. Comm.* **2011**, *13*, 3321−3324. (h) Xue, Y.-S.; He, Y.; Ren, S.-B.; Yue, Y.; Zhou, L.; Li, Y.-Z.; Du, H.-B.; You, X.-Z.; Chen, B. *J. Mater. Chem.* **2012**, *22*, 10195−10199. (j) Zhuang, W.; Yuan, D.; Liu, D.; Zhong, C.; Li, J.-R.; Zhou, H.-C. *Chem. Mater.* **2012**, *24*, 18−25.

(4) (a) Kitagawa, S.; Uemura, K. *Chem. Soc. Rev.* **2005**, *34*, 109−119. (b) Vittal, J. J. *Coord. Chem. Rev.* **2007**, *251*, 1781−1795. (c) Kawano, M.; Fujita, M. *Coord. Chem. Rev.* **2007**, *251*, 2592−2605.

(5) (a) Biradha, K.; Fujita, M. *Angew. Chem., Int. Ed.* **2002**, *41*, 3392−3395. (b) Pretsch, T.; Chapman, K. W.; Halder, G. J.; Kepert, C. J. *Chem. Commun.* **2006**, 1857−1859. (c) Bardelang, D.; Udachin, K. A.; Anedda, R.; Moudrakovski, I.; Leek, D. M.; Ripmeester, J. A.; Ratcliffe, C. I. *Chem. Commun.* **2008**, 4927−4929.

(6) (a) Liu, D.; Ren, Z.-G.; Li, H.-X.; Lang, J.-P.; Li, N.-Y.; Abrahams, B. F. *Angew. Chem., Int. Ed.* **2010**, *49*, 4767−4770. (b) Mir, M. H.; Koh, L. L.; Tan, G. K.; Vittal, J. J. *Angew. Chem., Int. Ed.* **2010**, *49*, 390−393.

(7) (a) Sharma, M. K.; Bharadwaj, P. K. *Inorg. Chem.* **2011**, *50*, 1889−1897. (b) Massera, C.; Melegari, M.; Kalenius, E.; Ugozzoli, F.; Dalcanale, E. *Chem.—Eur. J.* **2011**, *17*, 3064−3068. (c) Li, H.-X.; Ren, Z.-G.; Liu, D.; Chen, Y.; Lang, J.-P.; Cheng, Z.-P.; Zhu, X.-L.; Abrahams, B. F. *Chem. Commun.* **2010**, *46*, 8430−8432.

(8) Falkowski, J. M.; Wang, C.; Liu, S.; Lin, W. *Angew. Chem., Int. Ed.* **2011**, *50*, 8674−8678.

(9) (a) Ghosh, S. K.; Kaneko, W.; Kiriya, D.; Ohba, M.; Kitagawa, S. *Angew. Chem., Int. Ed.* **2008**, *47*, 8843−8847. (b) Ghosh, S. K.; Zhang, J. -P.; Kitagawa, S. *Angew. Chem., Int. Ed.* **2007**, *46*, 7965−7968.

(10) (a) Perles, J.; Iglesias, M.; Ruiz-Valero, C.; Snejko, N. *Chem. Commun.* **2003**, 346−347. (b) Perles, J.; Snejko, N.; Iglesias, M.; Monge, M. A. *J. Mater. Chem.* **2009**, *19*, 6504−6511.

(11) Song, Y.-M.; Luo, F.; Luo, M.-B.; Liao, Z.-W.; Sun, G.-M.; Tian, X.-Z.; Zhu, Y.; Yuan, Z.-J.; Liu, S.-J.; Xu, W.-Y.; Feng, X.-F. *Chem. Commun.* **2012**, *48*, 1006−1008.

(12) Bernini, M. C.; Gandara, F.; Iglesias, M.; Snejko, N.; Gutierrez-Puebla, E.; Brusau, E. V.; Narda, G. E.; Monge, M. A. *Chem.—Eur. J.* **2009**, *15*, 4896−4905.

(13) Cao, M.-L.; Mo, H.-J.; Liang, J.-J.; Ye, B.-H. *CrystEngComm* **2009**, *11*, 784−790.

(14) Xue, D.-X.; Zhang, W.-X.; Chen, X.-M.; Wang, H.-Z. *Chem. Commun.* **2008**, 1551−1553.

(15) Paz, F. A. A.; Klinowski, J. *Inorg. Chem.* **2004**, *43*, 3948−3954.

(16) *Digital Solutions for Imaging and Microscopy*, Version 3.1 for Windows; Soft Imaging System GmbH: Muenster, Germany, 1987−2000

(17) *SAINT-Plus*, Version 7.12; Bruker AXS Inc.: Madison, WI, USA, 2004.

(18) *XPREP2*, Version 6.14; Bruker AXS Inc.: Madison, WI, USA, 2003.

(19) Barbour, L. J. *J. Appl. Crystallogr.* **1999**, *32*, 351−352.

(20) Otwinowski, Z.; Minor, W. In *International Tables for Crystallography*; Rossman, M. G., Arnold, E., Eds.; Kluwer: Dordrecht, 2000; Vol. *F*.

(21) Sheldrick, G. M. *SADABS*; University of Gottingen: Germany, 1996.

(22) Sheldrick, G. M. *Acta Crystallogr.* **2008**, *A64*, 112−122.

(23) Spek, A. L. *J. Appl. Crystallogr.* **2003**, *36*, 7−13.

(24) Farrugia, L. J. *J. Appl. Crystallogr.* **1997**, *30*, 565−565.

(25) Macrae, C. F.; Bruno, I. J.; Chisholm, J. A.; Edgington, P. R.; McCabe, P.; Pidcock, E.; Rodriguez-Monge, L.; Taylor, R.; van de Streek, J.; Wood, P. A. *J. Appl. Crystallogr.* **2008**, *41*, 466−470.

(26) Yvon, K.; Jeitschko, W.; Parthé, E. *J. Appl. Crystallogr.* **1977**, *10*, 73−74.

(27) (a) Atwood, J. L.; Barbour, L. J.; Thallapally, P. K.; Wirsig, T. B. *Chem. Commun.* **2005**, 51−53. (b) Borel, C.; Davies, K.; Handa, P.; Hedberg, G.; Oliver, C. L.; Bourne, S. A.; Hakansson, M.; Langer, V.; Öhrström, L. *Cryst. Growth Des.* **2010**, *10*, 1971−1978.

(28) Barbour, L. J. *Absorbance Software*; University of Stellenbosch: Stellenbosch, South Africa.

(29) (a) Zhang, H.; Wang, F.; Kang, Y.; Zhang, J. *Inorg. Chem. Commun.* **2010**, *13*, 1429−1431. (b) Du, M.; Zhang, Z.-H.; Wang, X.-G.; Zhao, X.-J. *Inorg. Chim. Acta* **2009**, *362*, 1358−1360. (c) Furukawa, H.; Go, Y. B.; Ko, N.; Park, Y. K.; Uribe-Romo, F. J.; Kim, J.; O'Keeffe, M.; Yaghi, O. M. *Inorg. Chem.* **2011**, *50*, 9147−9152.

(30) Seo, J.; Matsuda, R.; Sakamoto, H.; Bonneau, C.; Kitagawa, S. *J. Am. Chem. Soc.* **2009**, *131*, 12792−12800.

(31) Cabeza, A. J. C.; Day, G. M.; Motherwell, W. D. S.; Jones, W. *Chem. Commun.* **2007**, 1600−1602.

(32) Chang, H.; Fu, M.; Zhao, X. J.; Yang, E. C. *J. Coord. Chem.* **2010**, *63*, 3551−3564.

(33) Zhu, S.; Zhang, H.; Zhao, Y.; Shao, M.; Wang, Z.; Li, M. *J. Mol. Struct.* **2008**, *892*, 420−426.